PNAS RESEARCH ARTICLE | EVOLUTION OPEN ACCESS

Long-term evolutionary persistence of a cryptic color polymorphism in frogs

Sandra Goutte[a,1] and Stéphane Boissinot[a,b,1]

Edited by Rasmus Nielsen, University of California Berkeley, Berkeley, CA; received December 11, 2024; accepted August 14, 2025

Color polymorphism can influence the evolutionary fate of cryptic species because it increases populations' chances of survival in heterogenous or variable environments. Yet, little is known about the molecular and evolutionary mechanisms underlying the persistence of cryptic color polymorphisms, or the impact these polymorphisms have on the macroevolutionary dynamics of lineages. Here, we examine the evolutionary history of the most widespread cryptic color polymorphism in anurans, involving green and brown morphs. Using an order-scale comparative analysis, we show that these morphs can coexist within species over long evolutionary periods and that polymorphic lineages switch habitat more frequently and have greater diversification rates than other groups. We then identify the locus responsible for the green/brown polymorphism in a group of African grass frogs, and demonstrate that it evolves under long-term balancing selection, resulting in trans-specific polymorphism. These results provide a microevolutionary mechanism for the long-term persistence of multiple color morphs within species observed at a macroevolutionary scale. This study underscores the importance of cryptic color polymorphism in the ecology and evolution of anurans, and provides a framework for future research on the genetic architecture and selective forces underlying cryptic coloration traits.

balancing selection | macroevolution | population genomics | animal coloration | Foxd3

Significance

Cryptic coloration enables animals to blend into their environments, reducing detection by predators or prey. In many species, multiple color morphs coexist, providing adaptive advantages in diverse habitats. However, the evolutionary mechanisms maintaining cryptic color polymorphism and its impact on species diversification remain poorly understood. Our study shows that in frogs, cryptic color polymorphism can persist over millions of years, and is associated with increased speciation and habitat shifts. These findings suggest that cryptic color polymorphism can influence the evolutionary trajectory of lineages by promoting dispersal into new ecological niches and enhancing population persistence in the face of environmental change.

Animals exhibit a wide variety of colors and patterns that play crucial roles in their survival by helping them avoid detection by visual predators. These cryptic color traits allow individuals to blend into their surroundings, masquerade as inanimate objects like leaves or bird droppings, or disrupt their body shape (1). The simultaneous occurrence of multiple color morphs within a species is common among cryptic-colored organisms, and similar color polymorphisms are found repeatedly across distantly related species (2, 3). Cryptic color polymorphisms have inspired much theoretical and empirical work aimed at resolving the apparent paradox of phenotypic and genetic variation persisting despite genetic drift and various selective pressures tending to reduce or eliminate it (4–9). Several evolutionary mechanisms such as variations in selection pressures across space or time (e.g., as a result of frequency-dependent predation), or heterozygote advantage, have been proposed (4, 10–16). Yet, in polymorphic populations, it is often unclear whether selective processes have maintained multiple color morphs over long evolutionary periods or if color polymorphisms represent a transient state where one of the morphs is on its way to fixation (17).

In anurans (frogs and toads), earthy tones that provide camouflage against vegetation or soil backgrounds are prevalent (18, 19). The most widespread form of color polymorphism in this group involves individuals displaying either a green, or a melanin-based, brown to gray, dorsal coloration—referred to hereafter as Green Color Polymorphism (GCP) (18, 19). Despite its commonness, the genetic basis and evolutionary mechanisms underlying anuran GCP remains poorly understood. To date, efforts to identify genetic loci associated with coloration in wild anuran populations have mostly focused on a handful of poison frog species, which display bright colors such as blue, red, or yellow, that serve aposematic and sexual signaling functions, and that are rarely found in other anurans (20–22). However, color traits' mode of inheritance has been established in a broader taxonomic range using crossing experiments (18). For instance, crosses have established that GCP is controlled by a single locus with a dominant *Green* allele in three North American frogs (23–25).

Here, we conduct an order-scale comparative analysis to retrace the evolution of GCP and show that this polymorphism can persist for long periods of evolutionary time and is associated with increased habitat transitions and diversification rates. We then investigate the genetic architecture of GCP in a radiation of African grass frogs endemic to the

Author affiliations: [a]Division of Science, New York University Abu Dhabi, PO Box 129188, Abu Dhabi, United Arab Emirates; and [b]Center for Genomics and Systems Biology, New York University Abu Dhabi, PO Box 129188, Abu Dhabi, United Arab Emirates

Author contributions: S.G. and S.B. designed research; S.G. performed research; S.G. analyzed data; and S.G. and S.B. wrote the paper.

The authors declare no competing interest.

This article is a PNAS Direct Submission.

PNAS policy is to publish maps as provided by the authors.

[1]To whom correspondence may be addressed. Email: sg5533@nyu.edu or sb5272@nyu.edu.

This article contains supporting information online at https://www.pnas.org/lookup/suppl/doi:10.1073/pnas.2425898122/-/DCSupplemental.

Published September 10, 2025.

Ethiopian Highlands (12 species; genus *Ptychadena*). Within this radiation, four species (*Ptychadena robeensis*, *Ptychadena levenorum*, *Ptychadena erlangeri,* and *Ptychadena nana*) form a monophyletic clade and share the same green/brown polymorphism (26). Using whole-genome resequencing data, we identify and characterize the GCP locus and show that this genomic region is evolving under long-term balancing selection, resulting in trans-specific polymorphisms. We discuss how the genomic architecture of the trait and species' ecology may play a role in the maintenance of cryptic color polymorphism, and how, in turn, GCP impacts the evolutionary fate of species carrying it.

Results

Green Coloration Evolves Rarely and Is More Evolutionarily Stable as a Polymorphic State. To retrace the evolution of green coloration in anurans, we examined 13,025 photos of 2,363 species for which phylogenetic information was available (27), representing 30.8% of species recognized at the time of writing (28) (Dataset S1). We categorized species as "Fixed green" (186 species), "Polymorphic" (191 species), and "Not green" (1,986 species), and fitted multiple k-states Markov models of evolution for the green coloration (*SI Appendix*, Fig. S1 and Table S1). We accounted for phenotype uncertainty by using a probability function based on the number of photos examined for each species and incorporating the overall proportions of each category within our dataset as a prior. Models of evolution where transitions between the Fixed green, Polymorphic, and Not green states occur at different rates best fitted our data. Additionally, the goodness of fit of the model requiring an intermediate "Polymorphic" state (POLY model) was greater (although not significantly) than that of the model allowing direct transitions between the Fixed green and Not green states (ARD model; *SI Appendix*, Fig. S1 and Table S1). In both models, the rate of evolution of the green coloration (transition from Not green to Polymorphic) was 16 times lower than the rate of transition from Fixed green to Polymorphic. The rate of fixation of the green coloration was a fourth of that of its loss.

We estimated the number of changes between color states during the evolution of anurans based on 1,000 stochastic maps of the trait, allowing for all transitions to have different rates (Fig. 1 *A* and *B*). We estimated that green coloration evolved 126 times (95% CI: 106 to 145), was fixed 98 times (81 to 113) from a polymorphic state, and was lost 388 times (332 to 440). Across the phylogeny, the average evolutionary time spent in the Polymorphic state was greater than in the Fixed green state (Fig. 1*C*). These results reveal that GCP can persist over long periods of evolutionary time, which suggests the possible action of variation-maintaining selective forces.

Color Polymorphism Is Associated with Higher Habitat Transition Rates. To determine whether the evolution of GCP is driven by environmental factors, we assembled habitat data for 1,989 species and compared the fit from multiple models of joint evolution between coloration and habitat states. A habitat-dependent model for the evolution of green coloration provided the best fit for our data (Fig. 1*D* and *SI Appendix*, Table S2). As in our global model of evolution, the loss rate of green coloration was greater than its evolution rate, in all habitats. Interestingly, transition rates between habitats were higher in Polymorphic lineages compared to other groups. Overall habitat transition rate was 0.003 for "Green", 0.002 for Not green, and 0.005 for Polymorphic lineages (Fig. 1*D*). In particular, transition rates were the highest in GCP lineages that transitioned from terrestrial to arboreal-terrestrial (0.033), and from arboreal-terrestrial to arboreal (0.039). These results indicate that green coloration is differentially selected in different habitats, and that GCP may facilitate habitat transitions.

Diversification Rate Is Higher in Polymorphic Lineages. Theoretically, color polymorphism has the potential to facilitate speciation and reduce extinction risk (8, 17, 29), but few empirical studies have assessed the relationship between color polymorphism and diversification rate thus far (30–33). To test whether GCP is associated with increased diversification in anurans, we compared GCP-dependent and independent models of diversification, while accounting for a potential unsampled factor affecting diversification, fitted on the 5,242 species included in the largest molecular anuran phylogeny available, representing 68.3% of known taxa (27). A GCP-dependent model accounting for an unsampled variable with three hidden states best fitted our data (*SI Appendix*, Table S3). In this model, net diversification averaged across hidden states was greater in Polymorphic lineages (0.145 ± 0.035 lineage^{-1} My^{-1}) compared to Fixed green (0.105 ± 0.017 lineage^{-1} My^{-1}) and Not green groups (0.066 ± 0.018 lineage^{-1} My^{-1}; Fig. 2 and *SI Appendix*, Table S4).

To assess whether greater net diversification rates in GCP lineages were due to splits into monomorphic species (e.g., linked to local adaptation), we fitted a set of cladogenetic speciation-extinction (ClaSSE) models (*SI Appendix*, Table S5). Our best-fitting model estimated that, within GCP lineages, speciation events resulted in Polymorphic daughter species more often than in Fixed green or Not green ones (*SI Appendix*, Fig. S2 and Table S6). Additionally, green color loss occurs most often within species (anagenesis), while green color fixation may occur either within species or concomitantly with speciation events (anagenesis or cladogenesis; *SI Appendix*, Fig. S2). These results indicate that GCP is associated with an increased net diversification rate in anurans, with GCP being often maintained through speciation events.

Two Genomic Regions Are Associated with GCP in the African Grass Frog *P. robeensis*. Our macroevolutionary analysis indicates that GCP can persist for long periods of evolutionary time, suggesting that selection may maintain this polymorphism. In order to determine a possible role of selection, we focused on the African grass frog *P. robeensis*, where individuals within the same population exhibit either a green or a brown dorsal coloration (Fig. 3*A*). In this species, green and brown skins differ in their density of iridophores, a cell type containing crystals that reflect white-to-blue colors (Supp. Methods; *SI Appendix*, Fig. S3 and Table S7). Additionally, guanine crystals contained within the iridophores are longer, more aligned, and closer to one-another in green compared to brown skin, which may explain their difference in reflectance (34) (*SI Appendix*, Figs. S3–S5, Table S7, and *Supplementary text*).

We conducted a genome-wide association study (GWAS) to identify the genetic basis of GCP in *P. robeensis*, for which a chromosome-level reference genome is available. We obtained whole genome resequencing data from 100 *P. robeensis* (average 2.78× coverage), including 61 brown and 39 green individuals. We found a primary association peak on chromosome 7, located 52 kb upstream of the gene *FoxD3* between two known *FoxD3* enhancers, *Tarzan* and *Victor* (35) (Fig. 3*B*). Examination of this genomic region across the population established the full penetrance of the alleles, with the *Green* allele being dominant over the *brown* allele. Most green individuals are heterozygous, and all brown individuals are homozygous at this GCP-associated locus. Additionally, the *Green* haplotype carries a ~10 kb deletion adjacent to the

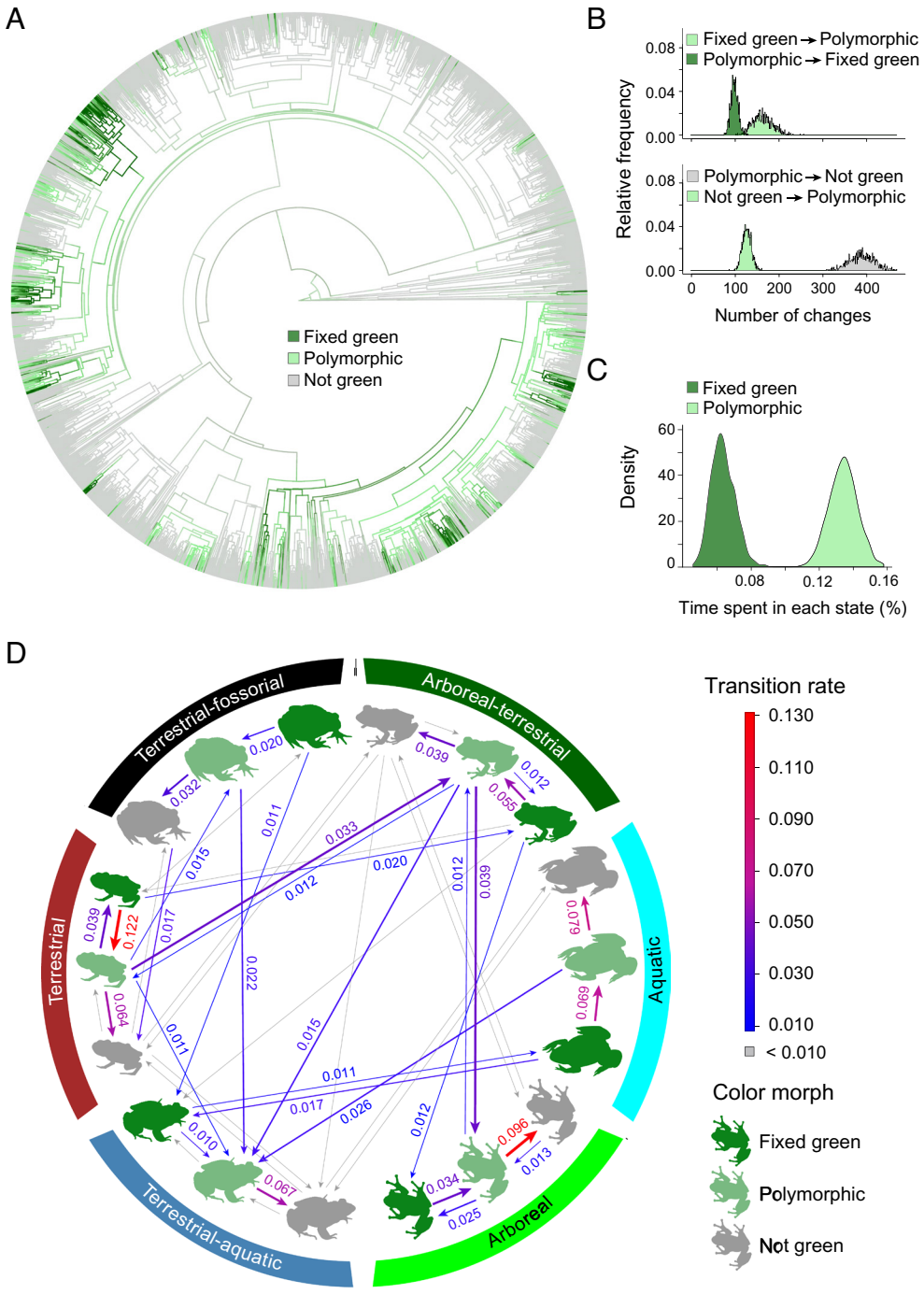

Fig. 1. Evolution of the green coloration and GCP in anurans. (*A*) Ancestral state reconstruction of the green coloration and GCP in 2,363 anurans (30.8% of known anuran species, all families represented; phylogeny from ref. 27) based on 1,000 stochastic maps using the POLY model of evolution. (*B*) Number of transitions between color states (Fixed green, Not green, and Polymorphic) during anurans' evolutionary history, estimated based on 1,000 stochastic maps. (*C*) Estimated time spent in Fixed green and Polymorphic states during the evolutionary history of anurans, based on 1,000 stochastic maps. (*D*) Codependence of green coloration evolution and habitat transitions in anurans. Transition rates estimated by the best fitting model of joint color and habitat evolution (see text) and above 0.010 are shown by the arrows.

association peak (Fig. 3*B*). The gene *FoxD3* is known to interact with the transcription factor *Mitf* (36) and is involved in iridophore differentiation in zebrafish, where an increase in *FoxD3* expression leads to differentiation of chromatophore precursors into iridophores instead of melanophores (37). We also found a secondary peak on chromosome 8 located within an intron of *Aox1*, a gene involved in the pteridine pathway. In zebrafish, *Aox5* (an *Aox1* orthologue) is a xanthophore marker known to interact with both *FoxD3* and *Mitf* (38). In this species, increased *Aox5* expression has been linked to enhanced proliferation of progenitor pigment cells (39). Thus, given the location of our association peaks near known *FoxD3* enhancers and within *Aox1*, as well as their known interactions in zebrafish, we hypothesized increased expression of both genes in the skin of green frogs.

FoxD3 Is Differentially Expressed in Green versus Brown Skin. We compared *FoxD3* and *Aox1* expression levels in the green and brown dorsal skin of 33 *P. robeensis* individuals across four developmental stages: tadpole, metamorph, juvenile, and adult. For tadpoles and metamorphs, where adult coloration has not

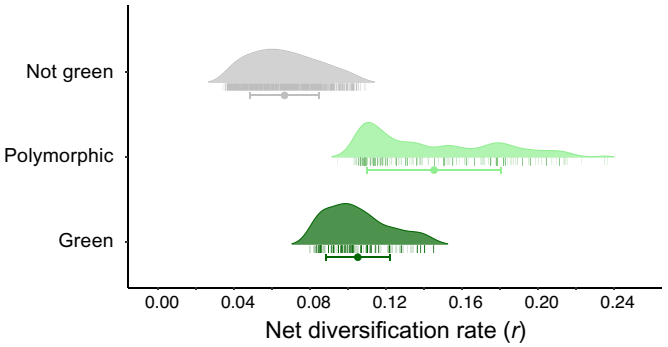

Fig. 2. GCP-dependent diversification rates in anurans. Distribution of tip-estimates of net diversification rates averaged across hidden states in Fixed green, Polymorphic, and Not green lineages under the MuHiSSE-3 model (see text and *SI Appendix*, Table S3). Full circles and horizontal bars show the mean and SD across tips, and vertical bars show the individual rates.

developed, we examined whole-genome resequencing data and used their genotype at the GCP locus to predict future coloration. *FoxD3* expression was higher in green versus brown-genotyped individuals across all developmental stages, and was overall higher in developing frogs compared to adults (Fig. 3*C* and *SI Appendix*, Table S8). The expression of *Aox1*, however, was not significantly different between the two groups (*SI Appendix*, Table S8). Additionally, we compared expression levels between skin patches in the vertebral stripe that were or would become green, with skin patches of the same individuals outside of the stripe that were and would remain brown (n = 14; Fig. 3*D*). We found that *FoxD3* expression was elevated in the skin that was or would become green but not in the areas that would remain brown (*SI Appendix*, Table S8). In contrast, while expression of *Aox1* differed significantly between green and brown skin patches within the same individuals, there was no difference between the green and brown skin across individuals when comparing the same skin patches (within or outside the stripe; *SI Appendix*, Table S8). Finally, we found that *FoxD3* and *Aox1* expression levels were positively correlated across samples (R = 0.64, $P < 0.001$; *SI Appendix*, Fig. S6). These results indicate that an increase in *FoxD3* expression level is associated with the appearance of green coloration *in P. robeensis*, while *Aox1* expression is spatially modulated within green individuals but does not appear to be directly linked to color determination.

The Green and Brown Alleles Are Maintained by Balancing Selection in *P. robeensis*. The simultaneous occurrence of two alleles within a species could be the result of incomplete fixation

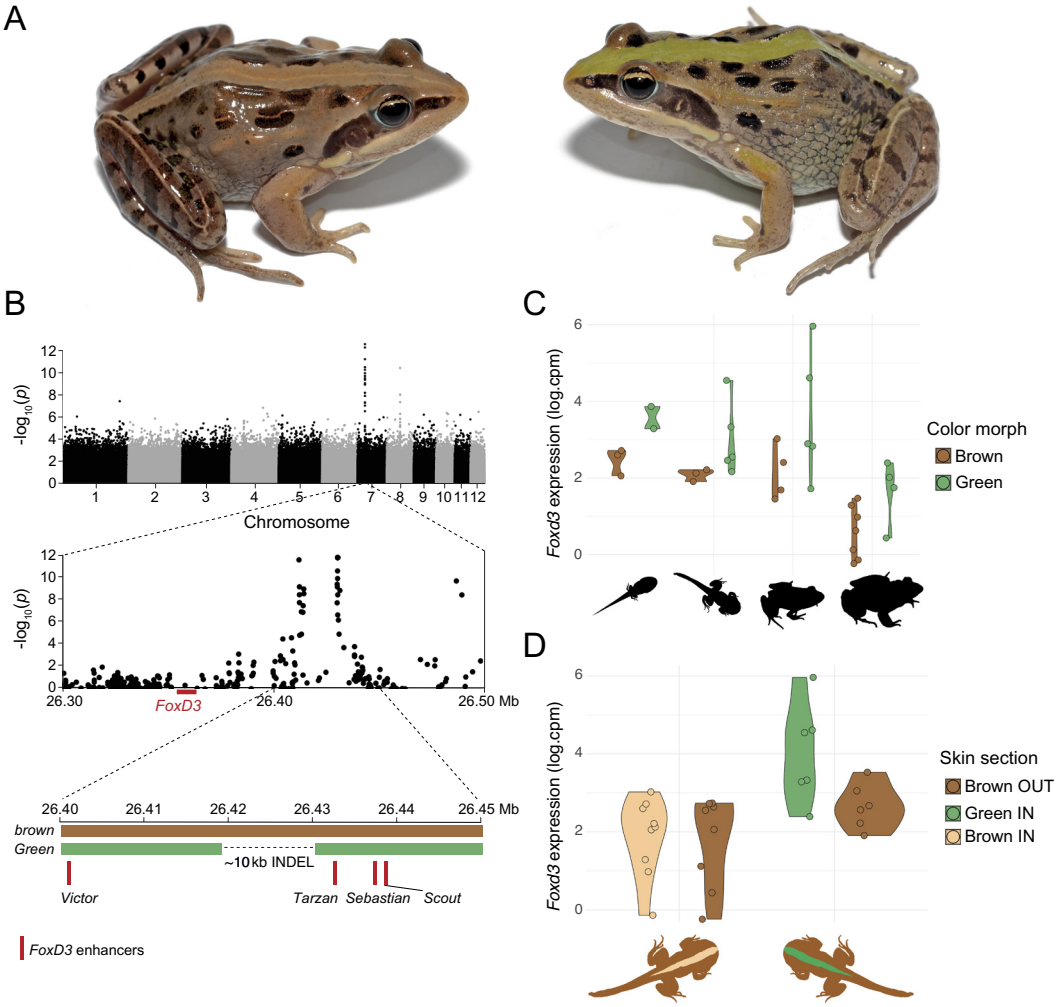

Fig. 3. A locus near *FoxD3* is associated with dorsal coloration in *P. robeensis*. (*A*) Brown (*Left*) and green (*Right*) morphs in *P. robeensis*. (*B*) Genome-wide association study of dorsal coloration in *P. robeensis* contrasting brown (n = 61) with green individuals (n = 39). The *Green* and *brown* alleles, as well as the known *FoxD3* enhancers in the region are represented below the Manhattan plots. (*C*) Expression levels of *FoxD3* in dorsal skin of *P. robeensis* (n = 33) with green and brown genotypes at different development stages. From left to right: tadpole (three brown, two green), metamorph (three brown, five green), juvenile (four brown, five green), and adult (seven brown, four green). (*D*) Expression levels of *FoxD3* in dorsal skin of *P. robeensis* (n = 28) in wide-striped, green and brown genotyped frogs within (eight brown, six green) and outside (eight brown, six green) the stripe.

of one of the alleles or could be maintained by balancing selection through heterozygote advantage, negative frequency-dependent selection, or heterogeneity in selection pressure across time or space (40). Balancing selection, if ancient enough, leaves genomic signatures distinguishable from other evolutionary processes (41). We searched for signatures of selection in the genome of *P. robeensis* using data from 10 frogs sequenced at higher-coverage (8.33×). We found a peak of genetic diversity (π) at the GCP locus in green individuals (mostly heterozygotes), while sequences in that region were all nearly identical in the brown frogs (Fig. 4*A*). The GCP locus association peak also coincided with a peak in absolute sequence divergence (D_{XY}) and genetic differentiation (F_{ST}) between the two morphs (Fig. 4 *B* and *C*), suggesting an ancient divergence of the two alleles. We then computed two statistics to scan for signatures of balancing selection specifically, Tajima's D, which compares the number of segregating sites and nucleotide diversity in a genomic region (42), and β, which is based on correlations of allele frequencies across neighboring loci (43). Tajima's D was positive across the GCP locus, indicating an increase in intermediate frequency polymorphism, which is consistent with balancing selection, although values were comparable to variation in the surrounding regions (Fig. 4*D*). We also found a peak of β scores (above the 99th genome-wide percentile) matching our primary association peak (Fig. 4*E*). The secondary association peak, however, did not coincide with a peak of genetic differentiation (F_{ST}) or β scores, although genetic diversity (π) and sequence divergence (D_{XY}) between green and brown individuals were elevated in this region (*SI Appendix*, Fig. S7). These results strongly suggest that, while unlikely at the *Aox1 locus,* long-term balancing selection is acting on the GCP locus, maintaining the *Green* and *brown* alleles in *P. robeensis.*

Local suppression of recombination can be instrumental for the persistence of balanced polymorphisms by preserving the integrality of divergent haplotypes generation after generation (40). This phenomenon is observed, for example, in alleles originating in chromosomal inversions (3, 40, 44). Surprisingly, in *P. robeensis*, we found an elevated recombination rate at the GCP locus compared to the chromosome-wide average (*SI Appendix*, Fig. S8). This pattern could reflect the long divergence time between the alleles, during which nucleotide diversity may have accumulated in the region surrounding the selected locus (45).

Long-Term Balancing Selection Maintains Trans-Species Color Polymorphism in the Ethiopian Highlands Grass Frog Radiation. To establish how long balancing selection has maintained color polymorphism in the Ethiopian Highlands grass frog radiation, we investigated whether the alleles found in *P. robeensis* were shared with the other three polymorphic *Ptychadena* species of the clade (*P. nana, P. levenorum,* and *P. erlangeri*). We found that variation at the GCP locus was associated with coloration in all three species, with a large number of shared nucleotide polymorphisms (*SI Appendix*, Fig. S9). Additionally, we found elevated nucleotide diversity (π) and sequence divergence (D_{XY}) between green and brown individuals at the GCP locus in all three species, as well as elevated F_{ST} between green and brown individuals for *P. nana* and *P. erlangeri* (*SI Appendix*, Fig. S10). We reconstructed a maximum-likelihood haplotype phylogeny of the GCP locus (3.38 kb; see *Material and Methods*) including all 12

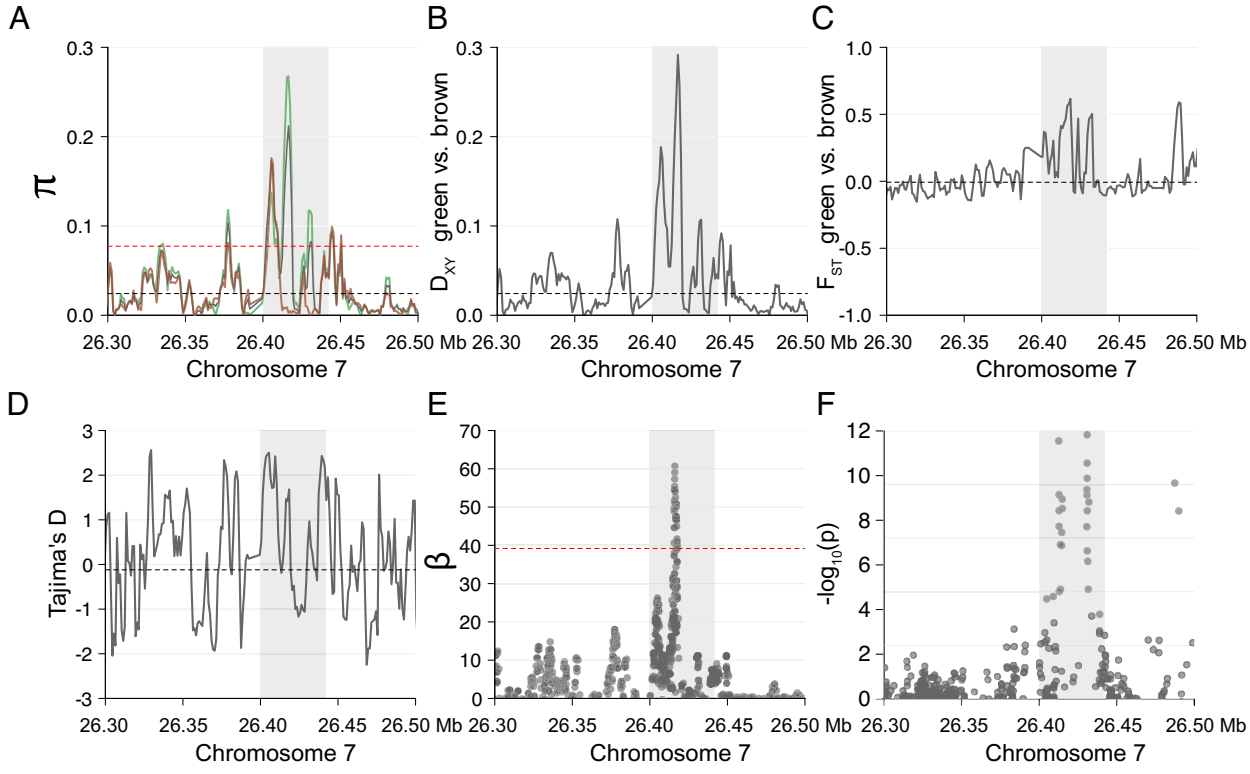

Fig. 4. Signatures of balancing selection in the GCP region of *P. robeensis*. All summary statistics (*A*–*E*) were computed on 3 kb sliding windows with 1 kb overlap on the higher-coverage dataset (n = 10, 8.33× average coverage). Gray-shaded areas correspond to the GCP-associated region (chromosome 7, position: 26,400,000 to 26,440,000). Black horizontal dashed lines represent the genome-wide average statistics' value. (*A*) Population-wide (gray), brown individuals (brown; all are homozygotes), and green individuals (green; most are heterozygotes) nucleotide diversity (π). The red horizontal dashed line represents the genome-wide 95th percentile of nucleotide diversity. (*B*) Absolute genetic divergence (D_{XY}) between green and brown individuals. (*C*) Relative differentiation (F_{ST}) between green and brown individuals. (*D*) Tajima's D values across the GCP region. (*E*) β scores. The red horizontal dashed line represents the genome-wide 99% percentile of β scores. (*F*) GWAS contrasting brown (n = 61) and green (n = 39) individuals.

species of the Ethiopian Highlands *Ptychadena* radiation (Fig. 5). The haplotype phylogeny shows a well-supported divergence of the *Green* and *brown* haplotypes, preceding the divergence of the four polymorphic *Ptychadena* species, estimated ~8 Mya (46) (Fig. 5). According to our phylogenetic reconstruction, the *Green* and *brown* haplotypes divergence even precedes the split between the *P. erlangeri* species group and the monomorphic (brown) *Ptychadena neumanni* species group, estimated ~9 to 10 Mya (46) (Fig. 5). This result represents strong evidence for ultra-long-term balancing selection (as defined in ref. 41) maintaining the *Green* and *brown* alleles in these four *Ptychadena* species.

Discussion

Widespread GCP in anurans allowed us to investigate the mechanisms maintaining cryptic color polymorphism at multiple scales, and evaluate its evolutionary consequences. Within the Ethiopian Highlands *Ptychadena* radiation, we showed that the green and brown color morphs have been maintained for millions of years by long-term balancing selection, leading to trans-specific polymorphism. At the order level scale, we found that GCP can persist for long periods of evolutionary time and is associated with frequent habitat transitions and high net diversification rates. Our results suggest that long-term balancing selection maintaining cryptic color polymorphism might be more prevalent than previously thought (41), and that GCP might play an important role in the ecoevolutionary fate of anuran species carrying it. Below, we discuss three aspects of our results: 1) how the genomic architecture of cryptic color traits may favor the maintenance of polymorphism through balancing selection, 2) the possible ecological drivers of this balancing selection, and 3) the macroevolutionary consequences of cryptic color polymorphisms maintenance in anurans.

The Genetic Architecture of GCP Favors the Maintenance of Polymorphism. How the genomic architecture of a trait influences its evolutionary fate and how selection, in turn, shapes the trait's genetic makeup is a fundamental question in evolutionary biology. If a polymorphic trait is governed by multiple, unlinked loci, high gene flow within a population is likely to produce intermediate, suboptimal morphs through recombination (40, 47). Single-locus architectures thus favor the maintenance of polymorphism. In *P. robeensis*, although two genes were associated with dorsal coloration, the genotype at the GCP locus fully explains the color morph. Variation at the second locus, located within *Aox1*, was found in some green *P. robeensis* individuals but was neither necessary nor sufficient to determine coloration, and was not found in the other polymorphic *Ptychadena* species. Dorsal coloration can therefore be considered governed by a single locus in this group, although, in *P. robeensis*, the two loci may be linked through epistasis involving a different, unmeasured trait.

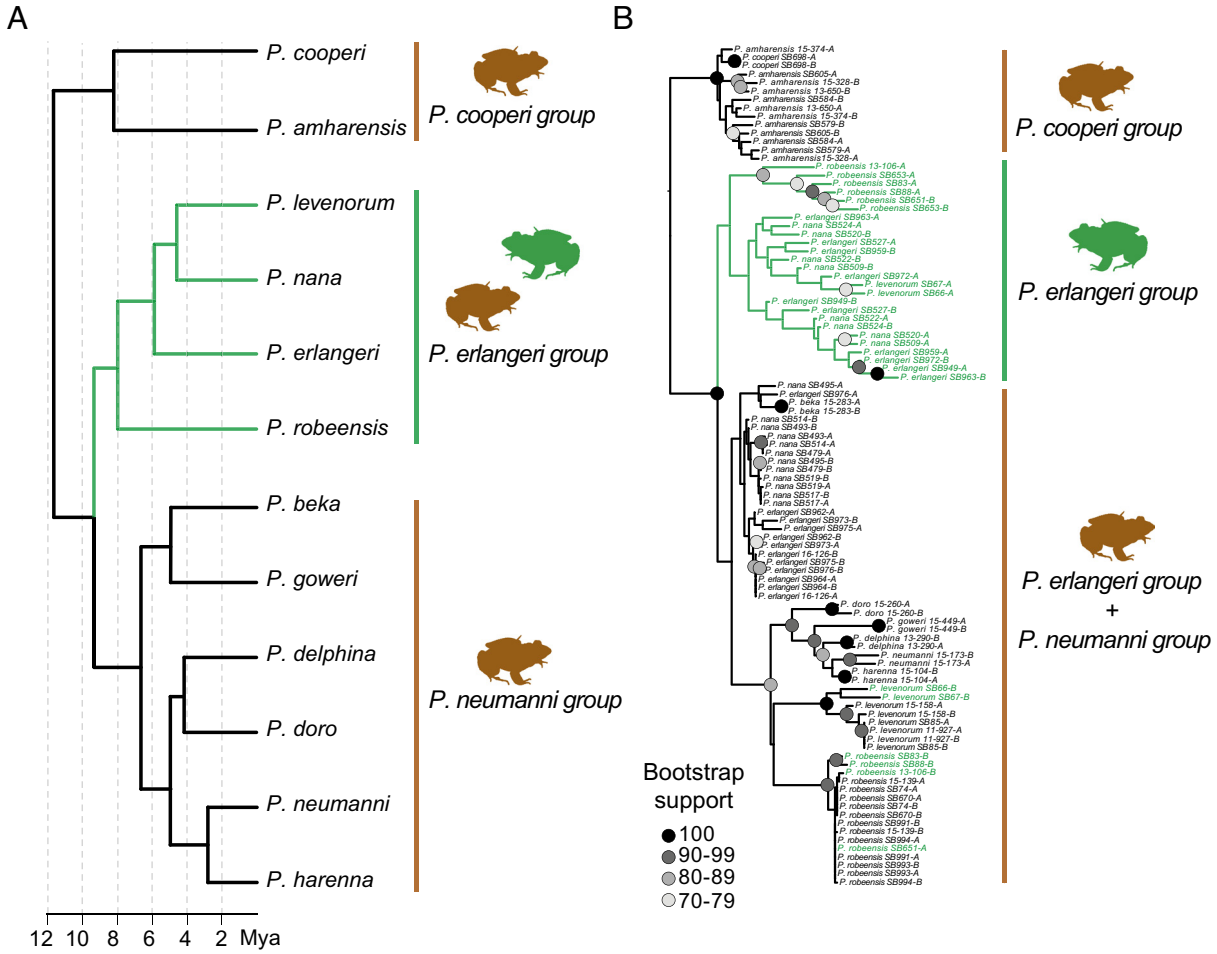

Fig. 5. The *Green* and *brown* alleles are under long-term balancing selection in four species of Ethiopian *Ptychadena*. (*A*) Species tree including all 12 species of the Ethiopian Highlands *Ptychadena* radiation with estimated divergence times, adapted from ref. 46. (*B*) Raxml-ng tree with 100 bootstrap iterations of the region of interest (3,383 bp; 762 SNPs after filtering) on the phased haplotypes of the 12 *Ptychadena* species. Haplotypes of individuals with a green phenotype are indicated in green. One of the haplotypes of four green *P. robeensis* and two green *P. levenorum* are grouped in the "brown" clade, indicating that those individuals are heterozygous at the GCP locus.

Dominance also impacts the probability of polymorphism maintenance. Because it is dominant over the ancestral *brown* allele, the newly evolved *Green* allele may have rapidly invaded an ancestral brown *Ptychadena* population if the green phenotype offered fitness benefits, particularly under negative frequency-dependent selection regimes, where rare phenotypes are selected for refs. 48 and 49. After the initial invasion, the dominance of *Green* over *brown* in turn would have promoted the maintenance of polymorphism within the population by preserving the recessive *brown* allele in heterozygotes, even if the green phenotype were under positive selection. The single-locus, dominant/recessive biallelic system determining dorsal coloration in the Ethiopian Highlands *Ptychadena* and in multiple other anuran species (23–25) thus represents a favorable genomic architecture for maintaining polymorphism. Being recessive, the *brown* allele is also more likely to become fixed when and where the brown phenotype is selected for. The prolonged maintenance of GCP, along with the high loss rate (from Polymorphic to Not green) and low fixation rate (from Polymorphic to Green) of the green coloration observed in our macroevolutionary analysis are therefore consistent with balancing selection acting on a single-locus *Green*-dominant/*brown*-recessive trait across anurans.

Possible Ecological Drivers of Balancing Selection in the Ethiopian Highlands Grass Frogs. Even with a favorable genomic architecture, long-term maintenance of polymorphism is considered unlikely because directional selection and drift are expected to lead to the fixation or loss of any allele over time (50). The maintenance of the *Green* and *brown* alleles over millions of years of divergence and multiple speciation events in *Ptychadena* thus represents strong evidence for long-term balancing selection. Differential selective values of alternative morphs across space and/or time constitutes the simplest explanation for balanced cryptic color polymorphism in natural populations (6, 51, 52). As selection by visual predators is expected to impose a strong pressure on anuran cryptic color evolution (18), predators' cognition and the level of crypsis in a given habitat should predict color morphs' adaptive values at any point in time and space, and may explain the simultaneous presence of multiple morphs within a population. Individuals of all four polymorphic Ethiopian Highlands *Ptychadena* inhabit heterogenous habitats consisting of grasslands and cultivated fields, and are found on brown (soil, mud) or green (grass) substrates, where the green and brown morphs offer different levels of crypsis. Predators of these species likely include birds and mammals, which can form searching images and may favor commonly encountered morphs, leading to apostatic selection (6). Both ecological heterogeneity and negative frequency-dependent selection by visual predators promote cryptic color polymorphism in prey (51), and may thus explain the maintenance of the green and brown morphs within populations in the *P. erlangeri* species group, although experimental data would be needed to confirm this hypothesis.

Balancing selection may also act upon other trait(s) correlated with GCP by pleiotropy. Traits that have been found to be associated with color morphs in anurans include female fecundity (53), overwinter survival (54), immunity (10), and larval development rate (55). In these systems, selection can act in opposite directions on the color trait and a pleiotropic trait, or two color-associated traits. For example, in the cricket frog *Acris crepitans,* individuals with the advantageous green- or red-striped morphs have lower immune capabilities compared to gray individuals, which may lead to balancing selection of the morphs (10). Polymorphism can also be maintained if heterozygotes have a fitness advantage compared to either homozygote. Heterozygote advantage can arise in genomic regions with low recombination and/or in which the alleles are old, because deleterious mutations may have accumulated on haplotypes underlying rare morphs, in particular if the haplotype is dominant and mostly found in heterozygotes (40). In the Ethiopian Highlands grass frogs, color polymorphism is associated with variation in the regulatory region of *FoxD3*, a gene not only involved in chromatophore differentiation, but also in neural crest development and autoimmune diseases in other vertebrates (37, 56). It is therefore possible that the *Green* allele, mostly found in heterozygotes, accumulated recessive mutations impacting other functions of *FoxD3* that are deleterious in homozygote *Green* individuals.

Ecological and Evolutionary Implications of Cryptic Polymorphism Maintenance in Anurans. In our macroevolution analysis, we found that GCP at the species level (including within and between-populations polymorphism) is associated with increased habitat transition rates, supporting the hypothesis that cryptic color polymorphism allows greater adaptability to novel ecological niches and could therefore promotes range expansion (8, 57). In agreement with classical ecological evolutionary theory (synthetized in refs. 8, 17, 29, and 58), we found a higher net diversification rate in GCP lineages compared to Fixed green and Not green groups. This result is consistent with an evolutionary scenario where colonization of new environments and biogeographic areas by polymorphic populations leads to greater speciation, and lower extinction rates. Several mechanisms can explain the relationship between GCP, habitat transition, and diversification. Speciation rate may increase when polymorphic populations become monomorphic in the process of colonizing new ecological niches, resulting in rapid divergence and reproductive isolation from ancestral populations (31). Cryptic color polymorphisms may also promote the persistence of populations under variable environmental conditions, which in turn lowers their risk of extinction (8, 57). Our results suggest the latter mechanism is more common than the former, although fixation of the green color may occur concurrently to speciation more often than its loss. Finally, rapid speciation may favor color polymorphism persistence by providing opportunities for the reintroduction of lost ancestral morphs through adaptive introgression, or their maintenance through the persistence of the ancestral selection regime in recently evolved daughter species (47).

To our knowledge, the association between color polymorphism and diversification rate at a macroevolutionary scale has only been examined in nonpasserine birds (31), Lacertidae lizards (30, 32), and carnivores (33) so far. These studies yield mixed results: in carnivores and three of the five bird families studied, accelerated speciation rates were linked to color polymorphism (33, 59), while in lacertids, two studies using the same species but different morph coding methods produced opposite results (30, 32). Interestingly, in birds of prey, where color polymorphism is associated with higher speciation rates, polymorphic species tend to have larger geographic ranges and occupy more diverse environments than monomorphic species (31). The clear patterns we obtained in our macroevolution and diversification analyses including 2,363 species across the order suggest that consistent forces drive the evolution and maintenance of GCP in anurans. These results provide a foundation for future research on how color polymorphism may facilitate dispersal to new ecological niches and enhance the survival of populations facing environmental changes.

Material and Methods

Order-Scale Comparative Analysis. We conducted a comparative analysis using the most recent molecular phylogeny for anurans, which comprises 5,242 species, representing all families and 68.5% of species recognized at the time of writing (27, 28). We collected data on dorsal coloration for 2,363 species, examining all photographs available for each species on Amphibiaweb (https://amphibiaweb.org). In a few cases, when no or few photos were available, we searched additional sources such as original species descriptions and the number of photographs examined for each species was systematically recorded (Dataset S1). In total, we examined 13,025 photos. Dorsal coloration (i.e., excluding thigh, ventral, or lateral coloration) was categorized as either Fixed green (green coloration always present), Not green (green coloration always absent), or Polymorphic (green coloration present in some individuals only). Frogs with translucent green coloration, such as the glass frog *Hyalinobatrachium vireovittatum* for example, were not coded as Fixed green or Polymorphic, since the color is known to be of different molecular origin and likely under different evolutionary processes (60). Photos in which dorsal coloration was unclear due to the photo's angle or illumination condition were removed from the analysis. Because phenotypes were coded at the species level, inter- and intrapopulation color polymorphisms were not distinguishable for this analysis.

To account for the possibility that polymorphic species were categorized as monomorphic due to a low number of examined individuals, we used the following probability function for species categorized as fixed green or Not green:

$$P\left(\text{polymorphic}_{\text{species}}|\text{green}_{\text{obs}}\right) = \frac{P\left(\text{polymorphic}_{\text{species}}\right) \times \left(\text{green}_{\text{obs}}|\text{polymorphic}_{\text{species}}\right)^{n}}{P\left(\text{green}_{\text{obs}}\right)},$$

Where $P(\text{polymorphic}_{\text{species}}|\text{green}_{\text{obs}})$ is the probability of a species categorized as Fixed green to be in fact polymorphic, $P(\text{polymorphic}_{\text{species}})$ is the probability of a species being polymorphic, $P(\text{green}_{\text{obs}}|\text{polymorphic}_{\text{species}})$ is the probability of a polymorphic species being categorized as Fixed green, $P(\text{green}_{\text{obs}})$ is the probability of categorizing a species as Fixed green, and n is the number of frogs examined. We used the overall proportion for each category in our dataset as priors, and gave a 50% chance to polymorphic species' individuals of being green. The probabilities for a given species sum to 1 across all categories, with, for example $P\left(\text{polymorphic}_{\text{species}}|\text{green}_{\text{obs}}\right) = P\left(\text{green}_{\text{species}}|\text{green}_{\text{obs}}\right)$ for pecies categorized as Fixed green. We used these probabilities as input phenotypic data in our analysis of green color evolution across anurans.

Habitat use data were collected independently for 1,989 species based on multiple large studies (61–64), species accounts in Amphibiaweb, and the IUCN red list websites as described in ref. 2 (https://amphibiaweb.org; https://www.iucnredlist.org; Dataset S1). We categorized anuran habitats as arboreal, aquatic, terrestrial, arboreal/terrestrial, terrestrial/fossorial, and terrestrial/aquatic, based on the main habitat occupied by adult individuals.

Evolution of the Green Coloration in Anurans. We fitted multiple k-stats Markov (Mk) models of evolution for the green coloration on our 2,363 species dataset and the accordingly pruned phylogeny from ref. 27 using the function *fitMk* in R package *phytools* (65). We compared four models of evolution: equal transition rates among Fixed green, Not green, and Polymorphic states (ER; one parameter), all transition rates different (ARD; six parameters), symmetric transition rates (SYM; three parameters), and a model allowing only transitions between green and not green through the Polymorphic state (POLY; four parameters). We compared the fit of our models by computing Akaike information criterion (AIC) and Akaike weights, and conducting pairwise likelihood ratio tests. The ARD and POLY models better fitted the data compared to the ER and SYM models. Goodness of fit was greater for the POLY compared to the ARD model, but it was not significantly different [Likelihood ratio test = 0.002 (df = 2), *P*-value = 0.999], and the estimated transition rates were equal in both models. We then reconstructed ancestral color states by creating 1,000 stochastic maps of the trait onto the phylogeny using the POLY model and the function *make.simmap* to estimate the number of transitions between states and the time spent in each state across the phylogeny.

Habitat-Dependent Evolution of the Green Coloration and GCP in Anurans. To assess whether the evolution of the green coloration and GCP were habitat-dependent, we first evaluated which model of evolution for habitat preference best fitted our data (*SI Appendix*, Fig. S11). We compared the goodness of fit of Mk models with all transition rates between habitats equal (ER; 1 parameter), all transition rates different (ARD; 30 parameters), transition rates different for each habitat pair but equal in either direction (SYM; 15 parameters). The ARD model better fitted our data compared to the ER and SYM models (*SI Appendix*, Table S9). In an attempt to reduce the number of estimated parameters, we compared three additional models representing reduced versions of the ARD model: the ordered model, allowing transitions between adjacent habitats (e.g., the transition fossorial-terrestrial -> arboreal was not allowed in this model). This model allowed the following transitions: arboreal <-> arboreal-terrestrial <-> terrestrial <-> terrestrial-aquatic <-> aquatic and terrestrial <-> fossorial-terrestrial (*SI Appendix*, Fig. S11). The two other models considered only transitions that were estimated ≥ 0.001 (Reduced model 1), and > 0.001 (Reduced model 2), in the ARD model. All models were fit on the 1,989 species dataset using the *fitMk* function. The reduced model 2 fitted our data substantially better than all other models (*SI Appendix*, Fig. S12 and Table S9), we thus used this model in subsequent analyses.

To test for coevolution between color states and habitats, we created a variable combining both variables for each species (e.g., "Fixed green + Arboreal", "Polymorphic + Terrestrial", etc.), while accounting for uncertainty of the color state. We then fitted multiple models of evolution using the *fitMk* function. To limit the number of estimated parameters, we only allowed transitions permitted in our best-fitting model for habitat evolution (reduced model 2), from Fixed green to Not green and vice-versa through the Polymorphic state, and did not allow simultaneous habitat and color states transitions (*SI Appendix*, Fig. S13). The most complete model allowed all transition rates to be different (FULL model; 60 parameters). Model 2 (16 parameters) allowed different transition rates between habitats and between color states, but habitat transition rates were equal across color states and color state transitions were independent of habitat. Model 3 (38 parameters) allowed all color state transition rates to be different within and across habitats, but transitions between habitats had the same rate regardless of the color state. Model 4 (40 parameters) allowed all color state transition rates to be different, but independent of habitat, and habitat transition rates to be all different and vary according to color state (*SI Appendix*, Fig. S13). We compared models' fit by computing their respective AIC and Akaike weights. The FULL model best fitted our data (*SI Appendix*, Table S2).

Color State-Dependent Diversification Analysis. To detect potential association between color states ("Fixed green, Not green, or Polymorphic) and diversification rate, we compared the goodness of fit of color state-dependent and color state-independent diversification models, while accounting for a potential unsampled variable with "hidden states" impacting diversification using the *MuHiSSE* function implemented in the R package *hisse* (66). For this analysis, we used the complete tree from ref. 27 comprising 5,242 anuran species and our full dataset of 2,363 characterized species. We fitted nine models: a model where diversification rate is independent of color states or hidden states (NULL; six parameters); a model in which diversification rate is dependent on color states but not on any hidden state (MuSSE; eight parameters); models where diversification rate is independent of color states but depends on a hidden variable with two to four states (CID-2; 8 parameters, CID-3; 9 parameters, CID-4; 10 parameters); models in which diversification rate depends on both color states and a hidden variable with 2 to 3 states, with transition rates between color states being independent of the hidden states (MuHISSE-2; 12 parameters, MuHISSE-3; 15 parameters); models with the same parameters but in which color state transition rates vary across hidden states (MuHISSEq-2; 16 parameters, MuHISSEq-3; 23 parameters). We compared the goodness of fit of our models by computing their respective AIC and Akaike weights (*SI Appendix*, Table S3).

To assess whether transitions from Polymorphic to Fixed green or Not green states occurred more often within species (anagenetic changes; e.g., resulting from drift or selection), or concomitantly with speciation events (cladogenetic changes; e.g., resulting from local adaptation or interruption of gene flow), we fitted five ClaSSE models implemented in the R package *diversitree* (67) to our data: a model where both anagenetic and cladogenetic changes can occur (CLADOANA; 13 parameters), a model where cladogenetic and anagenetic changes can

occur, but where a polymorphic species cannot give rise to two monomorphic daughter species (CLADO-ANA-2; 12 parameters), a model where transitions can occur only along the tree branches (ANA; 10 parameters), a model where transitions can only occur at the nodes of the tree (CLADO; 9 parameters), and a model where only cladogenetic changes can occur but a polymorphic species cannot give rise to two monomorphic daughter species (CLADO-2; 8 parameters; *SI Appendix*, Fig. S2). We compared the models by computing their respective AIC and Akaike weights (*SI Appendix*, Table S5). We then ran four Markov chain Monte Carlo runs for 1,000 generations and discarded the first 25% as burn-in for the CLADO-ANA-2 model, which best fitted our data. We assessed parameter estimates' convergence using Gelman and Rubin's diagnostic implemented in the R package *coda* (68). As all parameters had converged (diagnostic's upper CI ~ 1), we computed the posterior probabilities of the parameters of interest (*SI Appendix*, Fig. S2).

Sampling of Ethiopian Ptychadena. Individuals of the Ethiopian Highlands *Ptychadena* radiation were collected between 2011 and 2022. Our study was approved by the relevant Institutional Animal Care and Use Committee at Queens College and New York University School of Medicine (IACUC; Animal Welfare Assurance Number A32721–01 and laboratory animal protocol 19-0003). Frogs were sampled according to permits DA31/305/05, DA5/442/13, DA31/454/07, DA31/192/2010, DA31/230/2010, DA31/7/2011, and DA31/02/11 provided by the Ethiopian Wildlife Conservation Authority. We photographed individuals in life and exposed them to a lethal dose of benzocaine by ventral application of 20% benzocaine gel. We extracted tissue samples and stored them in RNAlater or 95% ethanol. Adult individuals were fixed in 10% formalin for 24 to 48 h, and then transferred to 70% ethanol. After preservation, we took additional photographs of all individuals. All specimens were deposited at the Natural History Collection of the University of Addis Ababa, Ethiopia. Tissue samples are deposited at the Vertebrate Tissue Collection, New York University Abu Dhabi (NYUAD).

***P. robeensis* Reference Genome.** The assembly of the de novo chromosome-level *P. robeensis* genome is available on GenBank under accession number GCA_036250615.1 and described in details in the *SI Appendix*. The assembled genome is 1.59 Gb in length and consists of 12 scaffolds containing 95.7% of bases, which corresponds to the haploid chromosome number reported in the genus *Ptychadena*, with an N50 of 157 Mb. Annotation was conducted using both gene prediction models and RNAseq reads from multiple tissues, and developmental stages (*SI Appendix*).

DNA and RNA Extractions and Sequencing. Genomic DNA of 120 *P. robeensis,* 10 *P. nana,* 15 *P. levenorum,* 11 *P. erlangeri,* 6 *P. amharensis* individuals, as well as of one individual of *Ptychadena beka, Ptychadena cooperi, Ptychadena delphina, Ptychadena doro, Ptychadena goweri, Ptychadena harenna,* and *P. neumanni,* was extracted from liver or muscle tissue using the DNeasy blood and tissue kit (Qiagen, Valencia, CA; *SI Appendix*, Tables S10 and S11). RNA was extracted from the skin of 33 *P. robeensis* individuals using a RNeasy mini kit (Qiagen, Valencia, CA). In this species, individuals can carry a thin (<0.6 mm wide in adults) or a wide (>1.6 mm wide in adults) stripe, or be unstriped (2). For 14 wide-striped individuals, RNA was extracted from dorsal skin within and outside the vertebral stripe separately. For all other individuals, RNA was extracted from dorsal skin (*SI Appendix*, Table S12). We quantified extracted DNA and RNA using a Qubit fluorometer (Life Technologies). DNA and RNA libraries were prepared using a NEB Ultra II FS DNA library prep kit and the NEB Ultra II RNA library prep kit in conjunction with the Poly(A) mRNA Magnetic isolation module, respectively, and sequenced on Illumina NextSeq 550 flow cells at the Genome Core Facility of NYUAD. After quality filtering, reads were aligned to the *P. robeensis* reference genome using *bwa-mem* (69). The average coverage of the *P. robeensis* genomic data was 2.78×, except for 10 individuals which we sequenced at an average of 8.33×. Other *Ptychadena* species were sequenced at an average of 6.80×, except for *P. delphina*, for which coverage was lower (3.50×). Variants were called using the function *HaplotypeCaller* from *gatk v3.5* (70). The low-coverage *P. robeensis* and higher-coverage *P. robeensis* together with the other *Ptychadena* samples were then combined and genotyped in two separate datasets using *CombineGVCF* and *GenotypeGVCFs* functions from *gatk*.

GWAS in *P. robeensis*. In order to remove potential hybrids or misidentified individuals from further analyses, we ran a SNPs PCA and an Admixture analysis on the low-coverage genomic dataset including 141 individuals identified as *P. robeensis* or *P. levenorum*, a closely related species with a partially overlapping distribution range (26) (*SI Appendix*). The final dataset comprised 100 individuals originating from a single population (*SI Appendix*, Fig. S14 and Table S10). We checked for individual relatedness using *PLINK 1.9* (63) and found no directly related individual pairs (all genetic relationship values were < 0.2). *P. robeensis* is polymorphic for both the vertebral stripe pattern (which can be thin, wide, or absent (26, 71) and the dorsal coloration (brown or green). We thus tested whether these two traits were linked in this species, and found no association [$\chi^2 = 0.168$ (df = 2), *P*-value = 0.92; *SI Appendix*, Table S13]. Finally, we conducted a GWAS on color morph using the score test (-doAsso2) function in *ANGSD* (72), which relies on genotype likelihoods rather than called genotypes–a more appropriate approach for low-coverage data compared to methods based on genotype frequencies. We retained only biallelic sites (-setMaxDiffObs 2), with no more than 20% missing data (-minInd 80), a quality > 30 (-minQ 30), a mapping quality > 20 (-minMapQ 20), and minor allele frequency > 0.05 (-minMaf 0.05). We visualized the result of the GWAS using the R package *qqman* (73).

FoxD3 and Aox1 Expression Analysis. RNAseq reads were aligned to the annotated reference genome using HISAT2 (74) and StringTie2 (75). A transcriptome-wide gene count matrix was then created using the script *prepDE.py3* provided on the StringTie website (https://ccb.jhu.edu/software/stringtie). Subsequent analyses were conducted in the *R* environment (76). We used the *R* package *edgeR* (77) to filter and normalize our data prior analysis. We filtered out genes which had a count below 1 count-per-million (cpm) in at least half of the samples, and applied a trimmed mean of M-values normalization of the data. We then calculated a contrast matrix and corrected for Poisson count noise using the *makeContrast* and *voom* functions of the R package *limma* (78), respectively. Developmental stage was introduced in the model as a covariate. We compared *FoxD3* and *Aox1* expression levels between green and brown individuals (n = 33, one sample per individual; see *SI Appendix*, Table S12), as well as between sections of dorsal skin within and outside the vertebral stripe within individuals (n = 14 individuals, two samples per individual; *SI Appendix*, Table S12), using the *eBayes* function (*SI Appendix*, Table S8). We also compared green and brown individuals within, and outside the stripe for wide-striped individuals (n = 14). Finally, we tested for coexpression of *FoxD3* and *Aox1* across samples using a Pearson's correlation test (*SI Appendix*, Fig. S6). For tadpoles and metamorphs, which do not display their adult coloration yet, we predicted adult coloration based on their GCP locus genotype.

Tests for Selection in *P. robeensis*. To detect potential signatures of selection acting on the GCP locus, we computed several population genomics statistics on our region of interest as well as across the entire genome using the higher coverage *P. robeensis* dataset (n = 10). We estimated overall and morph-specific nucleotide diversity (π), as well as intermorph sequence divergence (D_{XY}) and relative differentiation (F_{ST}) using *Pixy* (79). *Pixy* explicitly accounts for missing genotypes when computing genetic diversity statistics and therefore is more robust to missing data than other methods (79). As *Pixy* requires invariant sites information, we generated a VCF containing invariant sites using the *--all-sites true* option in the *GenotypeVCF* function of *gatk* (70). We filtered out sites with >40% missing data, and computed statistics over 3 kb sliding window with 1 kb overlap between windows.

To search specifically for signatures of long-term balancing selection, we used the summary statistics Tajima's D (42), as well as β of *BetaScan2* (43). Tajima's D tests for deviation from neutral molecular evolution by comparing the number of segregating sites and nucleotide diversity in a genomic region. Null Tajima's D values are consistent with neutral evolution, negative values indicate directional selection (positive or negative), and positive values indicate an increase in intermediate frequency polymorphism, consistent with balancing selection. We computed Tajima's D on a 3 kb sliding window with 1 kb overlap using *vcf-kit* (80). The β statistic, on the other hand, is useful to detect long or very long-term balancing selection [>25 $N_{ancestral}$ generations, where $N_{ancestral}$ is the effective population size of the ancestral population in which the alleles first appeared (81)]. Loci with β values above the 99th percentile of genome-wide values can be considered as likely to have experienced long-term balancing selection. We computed β across the entire genome on 3 kb windows in order to determine a threshold based on the top 1% β values and compared the β values in our region of interest to the threshold value.

Recombination Rate Mapping in *P. robeensis*. Balancing selection can be favored by local suppression or reduction of recombination rate due, for example, to a chromosomal inversion (3, 40, 44). To assess whether the maintenance of polymorphism at the GCP locus was favored by local reduction of recombination, we computed the recombination rate map along the genome using *LDhat* (82) and the higher-coverage *P. robeensis* dataset including ten individuals (8.33× average coverage). Sites with >50% missing data, and nonbiallelic sites were filtered out. We ran the *interval* program with a block penalty of five for 10,000,000 iterations, sampling every 5,000 iterations. We used a precomputed lookup table with parameters closest to our dataset (n = 50 haploid individuals and theta per site = 0.001) to generate a new lookup table using *lkgen*. We compared local recombination values at the GCP locus with the chromosome-wide average and 90th percentile values.

Comparative Genomics. Together with *P. robeensis*, three species (*P. nana, P. erlangeri,* and *P. levenorum*) form a monophyletic group within the Ethiopian *Ptychadena* radiation that shares the same green/brown polymorphism. We compared the genomic region corresponding to our association peaks in *P. robeensis* between green and brown individuals in all three species (*P. nana*: four green, six brown; *P. erlangeri*: five green, six brown; *P. levenorum*: two green, three brown). At the GCP locus, we found consistent variations between morphs across species, although our low sample size did not allow for a GWAS approach. We found multiple shared polymorphic sites across the four species concentrated in the region of our primary association peak in *P. robeensis* (Fig. 4*F*). The *Aox1* locus, on the other hand, was missing in other *Ptychadena* species (no reads aligned to the *P. robeensis* reference genome in this region), indicating that variation at this locus is private to *P. robeensis*.

We computed summary statistics along 3 kb sliding windows with a 1 kb overlap for all species using *Pixy* (79) and the same parameters as for *P. robeensis*. Similar to *P. robeensis*, all three species exhibited higher values of π and D_{XY} in the region of interest (*SI Appendix*, Fig. S10). F_{ST} values increased at the GCP locus in all species but *P. levenorum*, indicating a genetic differentiation between the two morphs in these species. The lower F_{ST} values in *P. levenorum* may be due to the lower sample size (n = 5) for this species compared to the other two (n = 10).

Because GCP locus haplotypes were not identical across species, and in order to establish their relatedness, we aimed to reconstruct a haplotype phylogeny. As the locus is intergenic and in order to determine the exact boundaries of the region with shared polymorphism, we conducted a topology weighting analysis including all four species and both green and brown individuals (eight groups in total) using *TWISST* (83). Topology weighting is a means to explore how relationships between groups of individuals (or haplotypes) vary across the genome. We phased the genomes of our four species using *Beagle* (84) with default parameters. We computed topology weighting on 50 SNPs overlapping sliding windows along chromosome 7. We then summed the weights for all topologies where green haplotypes grouped together across species versus where they did not, and plotted the summed weights. The summed weight of topologies grouping the green individuals together increased significantly in the region matching our association peak in *P. robeensis* (*SI Appendix*, Fig. S9). We used a 0.05 weight threshold to establish the boundaries of our region of interest, which was 3.38 kb in length. We then combined, genotyped, and phased the genomes of the 12 *Ptychadena* species of the radiation using the same parameters for *gatk* and *beagle*, and adding six *P. amharensis* individuals, as well as of one individual of *P. beka, P. cooperi, P. delphina, P. doro, P. goweri, P. harenna,* and *P. neumanni* to the previous dataset. Finally, we reconstructed a maximum likelihood phylogeny of this 3.38 kb genomic region for the phased haplotypes of our 12 *Ptychadena* species using *RaxML-NG* (85) and 100 bootstrap iterations. The region counted 762 SNPs after filtering out indels, nonbiallelic sites, low quality (Q < 30), and extreme depth coverage (DP < 2 and DP > 25).

Data, Materials, and Software Availability. Scripts used for the analyses of the data are available on GitHub (https://github.com/SandraGoutte/frog_color_polymorphism) (86). DNA and RNA sequences have been deposited in NCBI SRA (PRJNA1201793, PRJNA1206837, PRJNA1206835, PRJNA722913) (87–90).

ACKNOWLEDGMENTS. We thank Ethiopian Wildlife Conservation Authority and Ethiopian Biodiversity Institute for assistance with sampling and export permits. We are grateful to all the students, scientists, and local collaborators who have contributed to sample collection over the years, and, in particular, Abeje Kassie, Megersa Kelbessa, Itbarek Kibret, and Samuel Woldeyes. We also thank Marc Arnoux, Nizar Drou, Rachid Rezgui, Sneha Thomas, Rainer Straubinger, David Howse, and Sayel Daoud for lab assistance. Andrew Shantz, Mariana Lyra, and Theo Busschau, and two anonymous reviewers provided helpful comments on the manuscript. This project was funded by NYUAD Grant AD180 to S.B. Sequencing and microscopy were carried out using the Core Technology Platforms resources at NYUAD. Analyses were carried out using the High-Performance Computing resources at NYUAD. Bioinformatics assistance was provided by the NYUAD Bioinformatics Core at NYUAD, supported by the Center for Genomics and Systems Biology. This work was partially supported by Tamkeen under the NYU Abu Dhabi Research Institute Award to the NYUAD Center for Genomics and Systems Biology (ADHPG-CGSB).

1. G. D. Ruxton, W. L. Allen, T. N. Sherratt, M. P. Speed, *Avoiding Attack: The Evolutionary Ecology of Crypsis, Aposematism, and Mimicry* (Oxford University Press, 2018).
2. S. Goutte, I. Hariyani, K. Deroy Utzinger, Y. Bourgeois, S. Boissinot, Genomic analyses reveal association of ASIP with a recurrently-evolving adaptive color pattern in frogs. *Mol. Biol. Evol.* **39**, msac235 (2022), https://doi.org/10.1093/molbev/msac235.
3. D. Lindtke *et al.*, Long-term balancing selection on chromosomal variants associated with crypsis in a stick insect. *Mol. Ecol.* **26**, 6189–6205 (2017).
4. H. E. Hoekstra, K. E. Drumm, M. W. Nachman, Ecological genetics of adaptive color polymorphism in pocket mice: Geographic variation in selected and neutral genes. *Evolution* **58**, 1329–1341 (2004).
5. Y. Jin *et al.*, Population genomics of variegated toad-headed lizard *Phrynocephalus versicolor* and its adaptation to the colorful sand of the Gobi Desert. *Genome Biol. Evol.* **14**, evac076 (2022).
6. A. B. Bond, The evolution of color polymorphism: Crypticity, searching images, and apostatic selection. *Annu. Rev. Ecol. Evol. Syst.* **38**, 489–514 (2007).
7. P. Nosil, Reproductive isolation caused by visual predation on migrants between divergent environments. *Proc. Biol. Sci.* **271**, 1521–1528 (2004).
8. A. Forsman, J. Ahnesjö, S. Caesar, M. Karlsson, A model of ecological and evolutionary consequences of color polymorphism. *Ecology* **89**, 34–40 (2008).
9. E. B. Ford, Polymorphism. *Biol. Rev.* **20**, 73–88 (1945).
10. E. Nevo, Adaptive color polymorphism in cricket frogs. *Evolution* **27**, 353–367 (1973).
11. A. Rudh, A. Qvarnström, Adaptive colouration in amphibians. *Semin. Cell Dev. Biol.* **24**, 553–561 (2013).
12. J. Bourke, K. C. Busse, T. M. Bakker, Sex differences in polymorphic body coloration and dorsal pattern in Darwin's frogs (*Rhinoderma darwinii*). *Herpetol. J.* **21**, 227–234 (2011).
13. R. C. Bell, K. R. Zamudio, Sexual dichromatism in frogs: Natural selection, sexual selection and unexpected diversity. *Proc. Biol. Sci.* **279**, 4687–4693 (2012).
14. E. Twomey *et al.*, Phenotypic and genetic divergence among poison frog populations in a mimetic radiation. *PLoS One* **8**, e55443 (2013).
15. S. Stückler, X. I. Dawkins, M. J. Fuxjager, D. Preininger, From masquerading to blending in: Ontogenetic shifts in antipredator camouflage in Wallace's flying frogs. *Behav. Ecol. Sociobiol.* **77**, 102 (2023).
16. M. R. Muell, J. L. Brown, Integrating ecological niche modeling and rates of evolution to model geographic regions of mimetic color pattern selection. *Evol. Ecol.* **38**, 599–619 (2024).
17. S. M. Gray, J. S. McKinnon, Linking color polymorphism maintenance and speciation. *Trends Ecol. Evol.* **22**, 71–79 (2007).
18. E. A. Hoffman, M. S. Blouin, A review of colour and pattern polymorphisms in anurans. *Biol. J. Linn. Soc.* **70**, 633–665 (2000).
19. B. Rojas, Behavioural, ecological, and evolutionary aspects of diversity in frog colour patterns. *Biol. Rev.* **92**, 1059–1080 (2017).
20. C. L. Richards-Zawacki, I. J. Wang, K. Summers, Mate choice and the genetic basis for colour variation in a polymorphic dart frog: Inferences from a wild pedigree. *Mol. Ecol.* **21**, 3879–3892 (2012).
21. J. S. Vestergaard, E. Twomey, R. Larsen, K. Summers, R. Nielsen, Number of genes controlling a quantitative trait in a hybrid zone of the aposematic frog *Ranitomeya imitator*. *Proc. Biol. Sci.* **282**, 20141950 (2015).
22. A. M. M. Stuckert *et al.*, Variation in pigmentation gene expression is associated with distinct aposematic color morphs in the poison frog Dendrobates auratus. *BMC Evol. Biol.* **19**, 85 (2019).
23. J. C. Fogleman, P. S. Corn, D. Pettus, The genetic basis of a dorsal color polymorphism in Rana pipiens. *J. Hered.* **71**, 439–440 (1980).
24. W. F. Pyburn, Inheritance of the green vertebral stripe in *Acris crepitans*. *Southwest. Nat.* **6**, 164–167 (1961).
25. M. S. Blouin, Inheritance of a naturally occurring color polymorphism in the ornate chorus frog, *Pseudacris ornata*. *Copeia* **1989**, 1056–1059 (1989).
26. S. Goutte, J. Reyes-Velasco, X. Freilich, A. Kassie, S. Boissinot, Taxonomic revision of grass frogs (Ptychadenidae, *Ptychadena*) endemic to the Ethiopian highlands. *ZooKeys* **1016**, 77–141 (2021).
27. D. M. Portik, J. W. Streicher, J. J. Wiens, Frog phylogeny: A time-calibrated, species-level tree based on hundreds of loci and 5, 242 species. *Mol. Phylogenet. Evol.* **188**, 107907 (2023).
28. D. R. Frost, Amphibian species of the world: An online reference. (Version 6.1., American Museum of Natural History, New York, 2021). https://amphibiansoftheworld.amnh.org/index.php. Accessed 1 July 2022.
29. M. J. West-Eberhard, Alternative adaptations, speciation, and phylogeny (a review). *Proc. Natl. Acad. Sci. U.S.A.* **83**, 1388–1392 (1986).
30. K. M. Brock, E. J. McTavish, D. L. Edwards, Color polymorphism is a driver of diversification in the lizard family Lacertidae. *Syst. Biol.* **71**, 24–39 (2021).
31. A. F. Hugall, D. Stuart-Fox, Accelerated speciation in colour-polymorphic birds. *Nature* **485**, 631–634 (2012).

32. T. Solan, B. Sinervo, P. Geniez, P. David, P.-A. Crochet, Colour polymorphism and conspicuousness do not increase speciation rates in lacertids. *Peer Commun. J.* **3**, 1–18 (2023).
33. M. M. Heuer, K. Fischer, L. Tensen, Color polymorphic carnivores have faster speciation rates. *Sci. Rep.* **14**, 23721 (2024).
34. D. Gur *et al.*, In situ differentiation of iridophore crystallotypes underlies zebrafish stripe patterning. *Nat. Commun.* **11**, 6391 (2020).
35. S. Dimitrieva, P. Bucher, UCNEbase–A database of ultraconserved non-coding elements and genomic regulatory blocks. *Nucleic Acids Res.* **41**, D101–D109 (2013).
36. A. Kawakami, D. E. Fisher, The master role of microphthalmia-associated transcription factor in melanocyte and melanoma biology. *Lab. Invest.* **97**, 649–656 (2017).
37. K. Curran *et al.*, Interplay between Foxd3 and Mitf regulates cell fate plasticity in the zebrafish neural crest. *Dev. Biol.* **344**, 107–118 (2010).
38. K. Petratou, S. A. Spencer, R. N. Kelsh, J. A. Lister, The MITF paralog tfec is required in neural crest development for fate specification of the iridophore lineage from a multipotent pigment cell progenitor. *PLoS One* **16**, e0244794 (2021).
39. W. T. Frantz *et al.*, Pigment cell progenitor heterogeneity and reiteration of developmental signaling underlie melanocyte regeneration in zebrafish. *Elife* **12**, e78942 (2023).
40. V. Llaurens, A. Whibley, M. Joron, Genetic architecture and balancing selection: The life and death of differentiated variants. *Mol. Ecol.* **26**, 2430–2448 (2017).
41. B. D. Bitarello, D. Y. C. Brandt, D. Meyer, A. M. Andrés, Inferring balancing selection from genome-scale data. *Genome Biol. Evol.* **15**, evad032 (2023).
42. F. Tajima, Statistical method for testing the neutral mutation hypothesis by DNA polymorphism. *Genetics* **123**, 585–595 (1989).
43. K. M. Siewert, B. F. Voight, BetaScan2: Standardized statistics to detect balancing selection utilizing substitution data. *Genome Biol. Evol.* **12**, 3873–3877 (2020).
44. Z. Yan *et al.*, Evolution of a supergene that regulates a trans-species social polymorphism. *Nat. Ecol. Evol.* **4**, 240–249 (2020).
45. M. DeGiorgio, K. E. Lohmueller, R. Nielsen, A model-based approach for identifying signatures of ancient balancing selection in genetic data. *PLoS Genet.* **10**, e1004561 (2014).
46. M. L. Lyra, S. Kirchhof, S. Goutte, A. Kassie, S. Boissinot, Crossing the Rift valley: Using complete mitogenomes to infer the diversification and biogeographic history of Ethiopian highlands *Ptychadena* (anura: Ptychadenidae). *Front. Genet.* **14**, 1–13 (2023).
47. G. A. Jamie, J. I. Meier, The persistence of polymorphisms across species radiations. *Trends Ecol. Evol.* **35**, 795–808 (2020).
48. J. B. S. Haldane, A mathematical theory of natural and artificial selection, part V: Selection and mutation. *Math. Proc. Cambridge Philos. Soc.* **23**, 838–844 (1927).
49. S. Billiard, V. Castric, V. Llaurens, The integrative biology of genetic dominance. *Biol. Rev.* **96**, 2925–2942 (2021).
50. A. Fijarczyk, W. Babik, Detecting balancing selection in genomes: Limits and prospects. *Mol. Ecol.* **24**, 3529–3545 (2015).
51. A. B. Bond, A. C. Kamil, Spatial heterogeneity, predator cognition, and the evolution of color polymorphism in virtual prey. *Proc. Natl. Acad. Sci. U.S.A.* **103**, 3214–3219 (2006).
52. J. A. Allen *et al.*, Frequency-dependent selection by predators. *Philos. Trans. R. Soc. Lond. B Biol. Sci.* **319**, 485–503 (1988).
53. D. L. Jameson, S. Pequegnat, Estimation of relative viability and fecundity of color polymorphisms in anurans. *Evolution* **25**, 180–194 (1971).
54. D. J. Merrell, C. F. Rodell, Seasonal selection in the leopard frog, *Rana pipiens*. *Evolution* **22**, 284–288 (1968).
55. P. S. Corn, Field evidence for a relationship between color and developmental rate in the northern leopard frog (*Rana pipiens*). *Herpetologica* **37**, 155–160 (1981).
56. J. A. Schunter *et al.*, A novel FoxD3 variant is associated with vitiligo and elevated thyroid auto-antibodies. *J. Clin. Endocrinol. Metab.* **100**, E1335–E1342 (2015).
57. Y. Takahashi, S. Noriyuki, Colour polymorphism influences species' range and extinction risk. *Biol. Lett.* **15**, 20190228 (2019).
58. E. B. Ford, "Ecological genetics" in *Ecological Genetics*, E. B. Ford, Ed. (Springer, Netherlands, 1975), pp. 1–11.
59. I.-P. Chen, D. Stuart-Fox, A. F. Hugall, M. R. E. Symonds, Sexual selection and the evolution of complex color patterns in dragon lizards. *Evolution* **66**, 3605–3614 (2012).
60. C. Taboada *et al.*, Multiple origins of green coloration in frogs mediated by a novel biliverdin-binding serpin. *Proc. Natl. Acad. Sci. U.S.A.* **117**, 18574–18581 (2020).
61. S. D. Howard, D. P. Bickford, Amphibians over the edge: Silent extinction risk of data deficient species. *Divers. Distrib.* **20**, 837–846 (2014).
62. W. E. Duellman, L. Trueb, *Biology of Amphibians* (The John Hopkins University Press, 1994).
63. D. S. Moen, H. Morlon, J. J. Wiens, Testing convergence versus history: Convergence dominates phenotypic evolution for over 150 million years in frogs. *Syst. Biol.* **65**, 146–160 (2016).
64. M. Vidal-García, J. S. Keogh, Convergent evolution across the Australian continent: Ecotype diversification drives morphological convergence in two distantly related clades of Australian frogs. *J. Evol. Biol.* **28**, 2136–2151 (2015).
65. L. J. Revell, Phytools 2.0: An updated R ecosystem for phylogenetic comparative methods (and other things). *PeerJ* **12**, e16505 (2024).
66. J. M. Beaulieu, B. C. O'Meara, Detecting hidden diversification shifts in models of trait-dependent speciation and extinction. *Syst. Biol.* **65**, 583–601 (2016).
67. R. G. FitzJohn, Diversitree: Comparative phylogenetic analyses of diversification in R. *Methods Ecol. Evol.* **3**, 1084–1092 (2012).
68. M. Plummer, N. Best, K. Cowles, CODA: Convergence diagnosis and output analysis for MCMC (2006), vol. 6.
69. H. Li, Aligning sequence reads, clone sequences and assembly contigs with BWA-MEM. arxiv [Preprint] (2013). https://doi.org/10.48550/arXiv.1303.3997 (Accessed 10 April 2024).
70. A. McKenna *et al.*, The genome analysis toolkit: A MapReduce framework for analyzing next-generation DNA sequencing data. *Genome Res.* **20**, 1297–1303 (2010).
71. S. Goutte, J. Reyes-Velasco, A. Kassie, S. Boissinot, Genetic and morphometric analyses of historical type specimens clarify the taxonomy of the Ethiopian *Leptopelis gramineus* species complex (Anura, Arthroleptidae). *ZooKeys* **1128**, 63–97 (2022).
72. T. S. Korneliussen, A. Albrechtsen, R. Nielsen, ANGSD: Analysis of next generation sequencing data. *BMC Bioinformatics* **15**, 356 (2014).
73. S. D. Turner, Qqman: An R package for visualizing GWAS results using Q-Q and manhattan plots. *J. Open Source Softw.* **3**, 731 (2018).
74. D. Kim, J. M. Paggi, C. Park, C. Bennett, S. L. Salzberg, Graph-based genome alignment and genotyping with HISAT2 and HISAT-genotype. *Nat. Biotechnol.* **37**, 907–915 (2019).
75. S. Kovaka *et al.*, Transcriptome assembly from long-read RNA-seq alignments with StringTie2. *Genome Biol.* **20**, 278 (2019).
76. R Core Team, R: A Language and Environment for Statistical Computing (Version 4.2.2, R Foundation for Statistical Computing, Vienna, Austria, 2022).
77. M. D. Robinson, D. J. McCarthy, G. K. Smyth, edgeR: A Bioconductor package for differential expression analysis of digital gene expression data. *Bioinformatics* **26**, 139–140 (2010).
78. M. E. Ritchie *et al.*, Limma powers differential expression analyses for RNA-sequencing and microarray studies. *Nucleic Acids Res.* **43**, e47 (2015).
79. K. L. Korunes, K. Samuk, Pixy: Unbiased estimation of nucleotide diversity and divergence in the presence of missing data. *Mol. Ecol. Resour.* **21**, 1359–1368 (2021).
80. D. E. Cook, E. C. Andersen, VCF-kit: Assorted utilities for the variant call format. *Bioinformatics* **33**, 1581–1582 (2017).
81. V. Soni, J. D. Jensen, Temporal challenges in detecting balancing selection from population genomic data. *G3 (Bethesda)* **14**, jkae069 (2024).
82. G. McVean, P. Awadalla, P. Fearnhead, A coalescent-based method for detecting and estimating recombination from gene sequences. *Genetics* **160**, 1231–1241 (2002).
83. S. H. Martin, S. M. Van Belleghem, Exploring evolutionary relationships across the genome using topology weighting. *Genetics* **206**, 429–438 (2017).
84. B. L. Browning, X. Tian, Y. Zhou, S. R. Browning, Fast two-stage phasing of large-scale sequence data. *Am. J. Hum. Genet.* **108**, 1880–1890 (2021).
85. A. M. Kozlov, D. Darriba, T. Flouri, B. Morel, A. Stamatakis, RAxML-NG: A fast, scalable and user-friendly tool for maximum likelihood phylogenetic inference. *Bioinformatics* **35**, 4453–4455 (2019).
86. S. Goutte, Frog color polymorphism. GitHub. https://github.com/SandraGoutte/frog_color_polymorphism. Deposited 23 November 2024.
87. S. Goutte, Population genomics of Robe's grass frog (*Ptychadena robeensis*). NCBI:SRA. https://www.ncbi.nlm.nih.gov/sra/PRJNA1201793.
88. S. Goutte, Comparative genomics across the 12 species of the Ethiopian Highlands grass frog radiation (genus *Ptychadena*). NCBI:SRA. https://www.ncbi.nlm.nih.gov/sra/PRJNA1206837.
89. S. Goutte, Differential gene expression in the skin of *Ptychadena robeensis* across multiple developmental stages. NCBI:SRA. https://www.ncbi.nlm.nih.gov/sra/PRJNA1206835.
90. New York University Abu Dhabi, *Ptychadena robeensis* v1 Genome Assembly. NCBI:SRA. https://www.ncbi.nlm.nih.gov/bioproject?term=PRJNA722913.